Electrical Power and Energy Systems 107 (2019) 282–297

Contents lists available at ScienceDirect

Electrical Power and Energy Systems

journal homepage: www.elsevier.com/locate/ijepes

Hybrid renewable energy systems for household ancillary services

Lorenzo Bartolucci*, Stefano Cordiner, Vincenzo Mulone, Joao Luis Rossi

University of Rome Tor Vergata, via del Politecnico 1, 00133 Rome, Italy

ARTICLE INFO

Keywords:
Hybrid renewable energy systems
Microgrids
Fuel cells
Ancillary services
Renewables

ABSTRACT

The development of Hybrid Renewable Energy Systems (HRES) under the Distributed Generation (DG) paradigm is the support for substantial reduction of CO_2 emissions and for greater penetration of renewable energy sources. The performance and reliability of HRES depend on the interaction between demand, generation, storage and the energy management strategy. In this study a comparison between two different control strategies is presented. In particular, a Rule Based Control (RBC) strategy has been compared with a more sophisticated Model Predictive Control (MPC) for the management of an HRES for residential applications.

Results show that a HRES operating in a connected mode has potential to support grid balancing actions giving economic benefits for both end-users and providers. Moreover, the MPC strategy gives a potential reduction of the unbalanced energy exchange with the grid and a more efficient use of the HRES components. The MPC strategy allows thus for a more effective use of renewable sources if compared with a conventional RBC for a Microgrid of same size, thus allowing for a greater penetration of renewable sources into the energy mix, or equivalently, toward downsizing of storage and programmable source subsystems with economic benefits.

1. Introduction

1.1. Motivation and background

According to [1], the rapid industrialization over the past three decades due to globalization, new technologies and increased household energy consumption of the urban population has resulted in an unprecedented increase of the energy demand, and in particular electricity. This has led to the occurrence of a supply-demand gap in the power sector. The scarcity of non-renewable energy resources, rising of fuel prices, harmful emissions from fossil fuel combustion and the need for investments on infrastructure has given weak sustainability of energy production to meet the demand. As a possible solution, the Decentralized Energy Planning (DEP) has become one of the main alternatives considered. The evolution of the DEP paradigm is directly affected by five main factors, as reported by the IEA [2], and namely the developments in distributed generation technologies, the constraints on the construction of new transmission lines, the increased customer demand for highly reliable electricity, the electricity market liberalization and the concern about climate changes.

In this picture, micro-grids (MGs) can be considered as the "building blocks" of smart grids. In general, these are characterized by the integration of different DERs (Distributed Energy Resources), such as micro-turbines, photovoltaic (PV) arrays and other renewable or non-renewable sources together with energy storage systems (batteries, energy capacitors), as well as deferrable (e.g., electric vehicles) and non-deferrable loads at the distribution hierarchical level [3]. In a MG both demand-side and supply-side resources are allowed to exchange energy with the grid. From the customer's point of view, MGs may be a cheap alternative to supply both thermal and electric energy. On the other hand, from the grid's management point of view, a MG can be seen as a controlled unit within the power system operated as a single load/generator. The grid operator may send emergency signals to the MG(s) requesting an increase/decrease of the power supplies/demanded depending on the needs of the network, supporting the end-users to meet the requests through incentives. The interaction with the smart-building is key for the maximization of benefits, the bidirectional energy flux feature and data fluxes among those, enabling the collaboration of consumers as a "prosumers". The customer may thus act as a producer by selling the surplus of the energy produced toward the grid. The demand side actions for smart buildings in a microgrid focus are based on Demand Response (DR) strategies allowing for an interaction between the consumers and the utility [4,5].

Consumers can range from smaller scale such as residential apartments up to industrial buildings. In fact, during the last decade buildings have become major energy consumers over the world as they consume around 40% of the total end-use energy [6]. Thus, energy efficiency measures in buildings, including smart technologies and the

* Corresponding author.
E-mail address: lorenzo.bartolucci@uniroma2.it (L. Bartolucci).

https://doi.org/10.1016/j.ijepes.2018.11.021
Received 2 August 2018; Received in revised form 7 October 2018; Accepted 16 November 2018

Nomenclature

(PEM) FC	(Proton Exchange Membrane) Fuel Cell
AC	Alternative Current
BESS	Battery Energy Storage System
DC	Direct Current
DEP	Decentralized Energy Planning
DER(s)	Distributed Energy Resources
DG	Distributed Generation
DR	Demand Response
EMS	Energy Management System
ESS	Electric Storage System
HRES(s)	Hybrid Renewable Energy System(s)
LCOE	Levelized Cost Of Energy
MG(s)	Microgrid(s)
MGCC	Microgrid Central Coordinator
MILP	Mixed Integer Linear Programming
MPC	Model Predictive Control
MPPT	Maximum Power Point Tracker
PV	Photovoltaic
RBC	Rule Based Control
RES	Renewable Energy Sources

interaction with the smart-grid, are considered essential for the reduction of emissions and carbon footprint, supporting the RES penetration as well [7]. The need for an efficient Energy Management System (EMS) to supervise and monitor the energy fluxes in a building arises, whenever more than one energy source is used to supply a given load profile [8,9]. EMS and smart meters are two key components to implement effective DR control actions [10–12].

1.2. Literature overview

Few studies have been focused on the use of DR strategies for the optimization of given objectives under the control of EMS. In [13] an algorithm has been developed for optimal scheduling under dynamic thermal and electrical power profile constraints. The EMS developed considers a suitable thermal model to optimally program power consumption tasks. Özkan [14] presented a power management scheme with a Rule-Based Control (RBC) algorithm over smart electrical appliances to reduce electricity cost and smooth the peak of demand. Xue et al. [15] presented an interactive power demand management strategy for the thermal load of single buildings with a smart grid integrating renewable energy. Pascual et al. in [16] tested an energy management strategy in a full scale residential MG, by means of continuous operation under real conditions with the aim of minimizing peak and fluctuations of power exchanged with the main grid. Results show that the combination of electric and thermal storage systems with controllable loads is a promising technology to maximize the penetration level of renewable energies in the electric system. Several works have been proposed to evaluate the performance of multi-agent based optimization systems [17–19]. Yoo et al. in [17] proposed control schemes consisting of two layers of decision-making procedures. In the bottom layer, smart agents decide the optimal operation strategies of individual MG components. In the upper layer, the microgrid central coordinator (MGCC) manages multiple agents so that the MG can meet the load reduction requested by the grid operator. Lim et at [18] developed and tested a distributed load-shedding system for agent-based autonomous operation of a MG. Authors in [20] explored the peculiarities of a Fuzzy-logic controller for the management of wind turbine (WT) doubly fed induction generators with PV and fuel cell hybrid power sources system along with hydrogen storage hybrid energy system, showing the effective and robust operation of the proposed micro-grid in providing better power quality and uninterrupted service.

Model Predictive Control (MPC) strategies have been widely considered for efficiently optimizing MG operations while satisfying a time-varying request and operation constraints. In [21] the design of a MPC strategy has been proposed for efficient electric energy management in a domestic environment. They formalized the problem as a linear programming problem controlling the HVAC system to optimize a trade-off between user comfort and energy cost considering thermal comfort constraints. Authors in [22] used the MPC strategy dealing with the energy-water management in urban households to minimize the maintenance costs of the pump. The authors compared the open loop optimal control model and the closed-loop MPC showing the robustness of the latter in minimizing the pumping costs while meeting the customer demand. The method has been applied in [23] to an experimental MG located in Athens, Greece showing the feasibility and the effectiveness of the proposed approach. Chen et al. [24] used stochastic and robust optimization to evaluate the real-time price-based DR management for household applications. In [25], the authors used a Mixed Integer Linear Programming (MILP) framework for the development of house EMS applying a DR strategy and to design systems from a techno-economical perspective. In general, special focus needs to be paid to the control of the Electric Storage System (ESS) whenever PV, or other non-programmable renewable energy sources (RES) are used in the MG. In their analysis, Dagdougui et al. [26] adopted MPC for a system model integrated to a dynamic decision model to optimize a complex hybrid system with RES. Lu et al. [27] used a mixed-integer nonlinear programming approach to solve optimization scheduling problems of energy management systems in a building with integrated energy generation and thermal storage. The MPC has been successfully used to implement DR for building heating systems in several works [28] showing its robustness and feasibility to minimize the objective functions proposed. One of the key aspects to fully exploiting the MGs' potential highlighted by the abovementioned works is the feature of taking into account the intrinsic fluctuations of the RES availability [29] and of load demand.

1.3. Contribution of the paper

In the context depicted, this work is focused at evaluating the capabilities of a household HRES to serve also as ancillary service toward the grid. The demand profile has been accurately represented according to typical household standards, accounting for both thermal and electric load. Detailed and quantitative comparison in terms of unbalance energy exchanged with the grid and self-consumption index is proposed for a simple (RBC) and a more sophisticated (MPC) controlled HRES compared with a standard prosumer reference case. Weather and load forecasting techniques are used to pre-optimize in the EMS the energy fluxes of all the HRES sub-components to move the deferrable loads whenever high RES availability occurs. The minimization of the objective function to be targeted has thus been defined as a multi-purpose optimization procedure toward the increase of subsystems durability, operational costs and capabilities of providing ancillary services. The model has further been applied to understand the effect of system design (mainly sizing of the different subsystems) on performance, showing the potential of the proposed strategy for components downsizing.

2. Hybrid renewable energy system configuration

The Hybrid Renewable Energy System (HRES) considered for the analysis (Fig. 1) includes a PV power plant of 5 KWp, connected to the Direct Current (DC) bus via a Maximum Power Point Tracker (MPPT) charger and DC/DC converter, coupled with a 225 Ah battery energy storage system operating at a nominal voltage of 48 V. The Proton

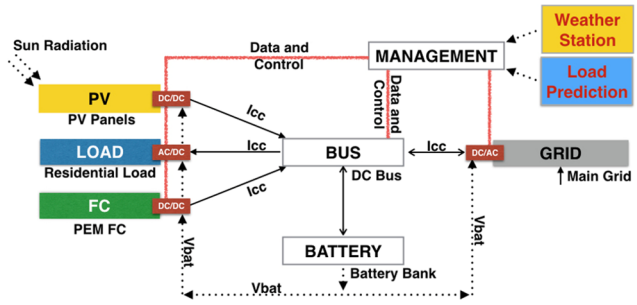

Fig. 1. MicroGrid (MG) layout.

Exchange Membrane Fuel Cell (PEM FC) has a power size of 1.2 kW at full load, connected to the DC bus via a DC/DC converter. The GRID is connected to the DC Bus via an AC/DC converter and has a peak power of 6 kW. The DC/DC and AC/DC converters were considered ideal for this test, i.e. losses have been neglected. The design of the HRES has been defined in previous works [30], where the details are reported. System sizing allows for minimizing the operational and installation costs referring to a standard Italian household load profile met with a Hybrid Renewable Energy System according to a RBC strategy. The design has been then perturbed, in the second part of the proposed work, to highlight room for further optimization.

Special focus has been given to the definition of the residential load, with typical Italian household characteristics and an energy consumption over the year of 4 MWh. Due to the lack of historical data, daily simulations of the load profile of a typical house have been carried out for a period of 4 years to define the expected load profile. The load profiles considered have been defined with a stochastic generator whose schematic is reported in Fig. 2 [31]. The load profile is generated depending on weather data and related probability to use a certain appliance. Then, a random number generator has been used to define the periods of operation of the different appliances according to both historical data and probability of use. The procedure has been repeated for each appliance in the household. Energy consumed by common appliances have been taken into account using real consumption profiles based on measurements carried out in [32] for lighting, electric boiler, electric oven, refrigerator, microwave oven, PC, TV, dishwasher, washing-machine and dryer. The residential load profile has been calculated for each day of the 4 simulated years and used as expected load in the EMS.

3. Control strategies

3.1. Rule-based control

The RBC strategy is based on a set of rules of priority use to supply current at the load, and further rules based on the current state of single sub-systems. More in detail, from the supply side, the PV power plant has priority over the battery pack, the FC and the GRID; on the other hand, from the demand side, the user load has priority over the battery pack in case of RES availability from the load consumption side. The subsystems are all connected in parallel to the DC-bus, and therefore the order of priority is given through the operating voltage of each component: the higher the value, the higher the priority. The voltage values used for the analysis are the same defined in previous studies [33–36].

In particular, four different set-point values have been set for the characterization of the system:

- **Vset1 –** is the minimum voltage allowed for the BESS discharge. It has been set at 46 V for the specific BESS technology used.
- **Vset2 –** is the nominal DC-bus voltage. Therefore it is the operative voltage for both grid and FC. For this study it has been set at 48 V.
- **Vset3 –** is the reference voltage value for the PV operation. It has been set at 49 V.
- **Vset4 –** is the floating voltage of the BESS that is set at 54 V.

A threshold power value to control the switch between FC and GRID has been defined. In particular the analysis of the Levelized Cost Of Energy (LCOE) tells that the FC system costs significantly drop at about 900 operating hours per year, slightly increasing beyond that (Fig. 3). The FC control strategy has thus been defined to have it activated only

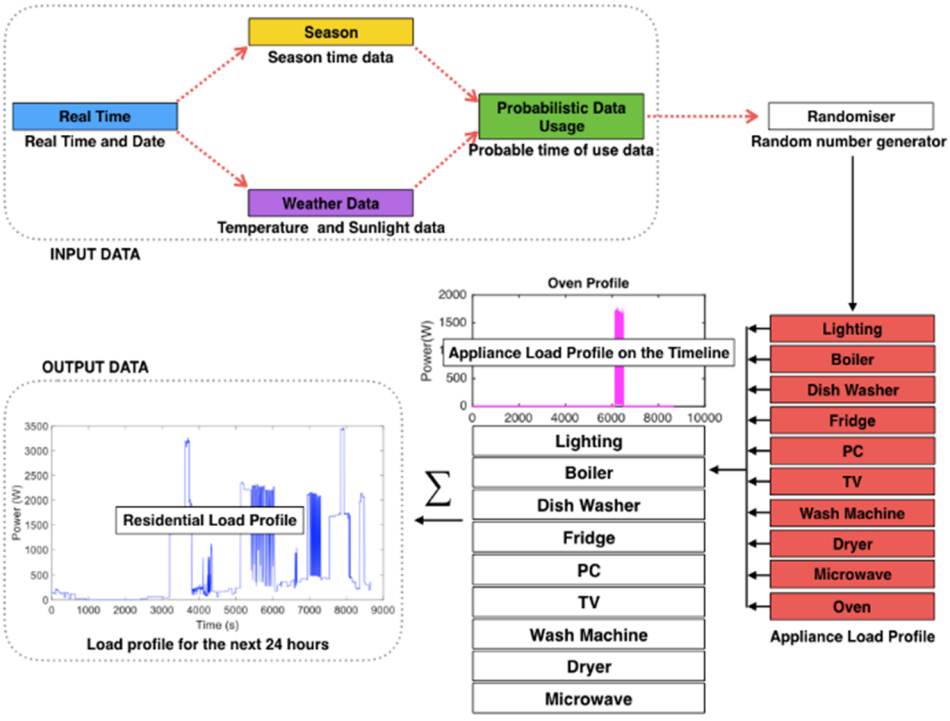

Fig. 2. Load generation model flow chart [31].

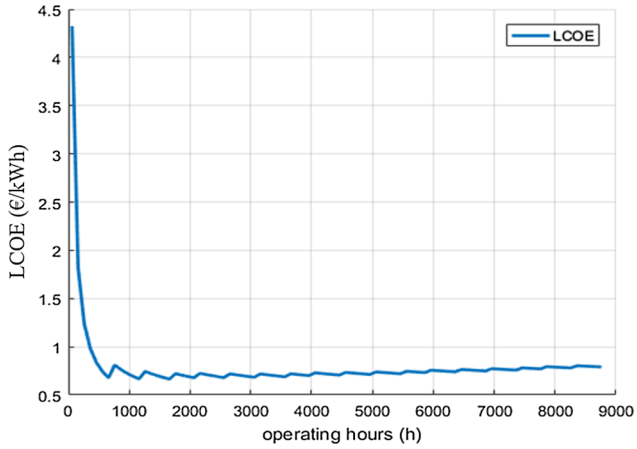

Fig. 3. Levelized Cost Of Energy as a function of Fuel Cell operating hours.

if:

$$P_{LOAD} - P_{PV} < X * P_{FC} \tag{1}$$

where P_{PV} is the actual power produced by the PV panels, P_{LOAD} is the load instantaneous requested by the users, P_{FC} is the nominal power of the FC and X is a parameter chosen to ensure approximately 900 h operation per year. Different simulations have been performed perturbing the FC size to evaluate X to obtain the desired FC operating hours. Results in terms of operating hours depending on X are reported in Fig. 4 according to different FC power sizes at equal P_{PV}.

The overall RBC strategy is schematized in the flow-chart reported in Fig. 5.

3.2. Model predictive control

The MPC strategy is operated through an optimization procedure defining control commands in order to minimize – or maximize – an objective function that is defined through modeling parameters.

The problem can be defined by a set of equations in the form:

$$x_{k+1} = Ax_k + Bu_k + B_d d_k + B_w w_k$$

$$y_k = Cx_k \tag{2}$$

where y_k is the output of the system, x_k is the current state, u_k is the control variable, d_k is an external disturbance and w_k represents uncertainties. The matrixes A, B, B_d, B_w and C model the system behavior.

Based on the initial state of the system and an estimation of the external uncertain variables (i.e. for this study the weather and the load), the MPC algorithm evaluates a set of control variables for a time period defined between t (current state) and t + CP (where CP is the control period). These control actions are then used to affect the behavior of the system at the time k + 1 as input for the next optimization process. The control variables are:

- the power purchased/sold from/to the grid;
- the power supplied by the FC;
- the binary variables required to control the system (e.g. to avoid frequent/repeated FC start-up/stand-by status or simultaneous energy sold/purchased to/from the grid);
- the commands to defer loads.

The effectiveness of the optimization process is highly dependent on the definition of the constraints and the objective function. The first are required in order to ensure physical and technical feasibility of the optimal solution found, while the latter defines the goals to be achieved. For this study a minimization of the operating costs, taking into account the unbalances, replacement, operating, and investment costs is proposed as a target of the controller system.

The MG has been modeled by means of the power balance equation here reported and implemented on a Matlab/Simulink based code:

$$\frac{dS}{dt} = P_{\text{pv}} + P_{\text{fc}} + P_{\text{grid}} - P_{\text{load}} \tag{3}$$

where S represents the energy stored in the battery pack, P_{pv}, P_{fc} are respectively the power produced by the photovoltaic plant, the output power of the fuel cell, while P_{grid} and P_{load} represent the power exchanged with the grid and the electric load requested by the house.

A Mixed Integer Linear Programming (MILP) algorithm has been used to solve the MPC strategy with a sampling time of 20 min over a rolling horizon mode to optimize a cost objective function in the form:

$$J^*(x_k) = \min_{u_{k|k} u_{k+1|k} \cdots u_{k+N-1|k}} V_f(x_{k+N|k}) + \sum_{i=0}^{N-1} l_i(x_{k+i|k}, u_{k+i|k}) \tag{4}$$

where l_i are the operating costs during the optimization phase, and V_f is the total cost of the system including maintenance during the period of operation. In this study all the operating (energy purchased from the grid, hydrogen cost, etc.) and capital costs have been considered as well as the revenue for the energy sold and the grid balancing actions (more details about definition of costs are reported in Section 4).

Technical constraints have been also implemented into the optimization procedure to ensure a smooth and regular operation of the system.

To increase battery durability, the state of charge has been enforced to range between 60% and 100% of the maximum battery charge (Smin, Smax).

$$\text{Smin} \leqslant \text{ST} \leqslant \text{Smax} \tag{5}$$

The power output of the fuel cell has been also limited into a given range; other constraints have been defined to avoid simultaneous operation of standby and operating mode and to count the number of FC start-ups to be taken into account into the cost function. The general formulation of the constraints is here reported:

$$P_{\text{FC|t}} - P_{max} \times \delta_{\text{on/off|t}} \leq 0 \tag{6}$$

$$-P_{\text{FC|t}} + 300 \times \delta_{\text{on/off|t}} \leq 0 \tag{7}$$

$$\delta_{\text{on/off|t}} + \delta_{\text{standby|t}} \leq 1 \tag{8}$$

$$\delta_{\text{on/off|t}} + \delta_{\text{standby|t}} + \delta_{\text{startup|t}} - \delta_{\text{on/off|t-1}} - \delta_{\text{standby|t-1}} = 0 \tag{9}$$

The grid has been modeled similarly. To limit the maximum power at 3000 W in both directions and to avoid simultaneous positive and negative power flow, the following constrains have been defined:

$$P_{\text{fromgrid|t}} - 3000 \times \delta_{\text{fromgrid|t}} \leq 0 \tag{10}$$

$$P_{\text{togrid|t}} - 3000 \times \delta_{\text{togrid|t}} \leq 0 \tag{11}$$

$$\delta_{\text{fromgrid|t}} + \delta_{\text{togrid|t}} \leq 1 \tag{12}$$

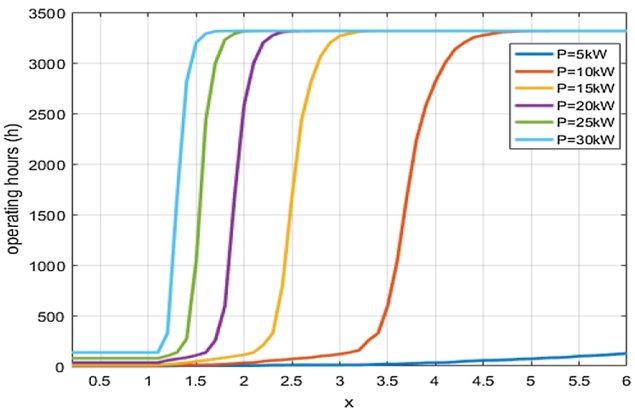

Fig. 4. Fuel Cell operating hours as a function of the parameter X in Eq. (1).

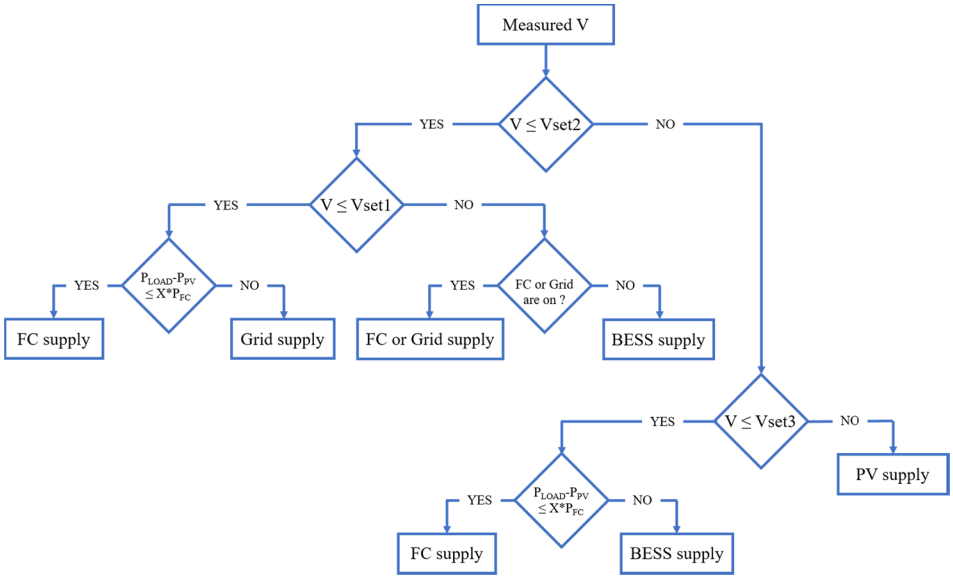

Fig. 5. RBC strategy flow-chart.

$$P_{\text{fromgrid}|t},\ P_{\text{togrid}|t},\ P_{\text{unb}^+|t},\ P_{\text{unb}^-|t} \geq 0 \tag{13}$$

$$P_{\text{fromgrid}|t} - P_{\text{togrid}|t} + P_{\text{unb}^+|t} - P_{\text{unb}^-|t} = P_{\text{gridref}|t} \tag{14}$$

The last equation forces the grid exchange power profile to attend the reference one; in case it cannot be maintained, two variables (Punb + |t, Punb − |t) are defined to apply corresponding costs. The reference function Pgridref|t can be defined according to an expected production from renewables. For control purposes it may thus be assumed that a minimization of the unbalance power needs to be pursued.

Three appliances have been implemented as controlled deferrable loads, namely the dishwasher, the washing machine and the dryer; it is further considered that a shift of their start-up within 24 h from the activation signal will not affect significantly the comfort of the end-user. Each appliance has been modeled by means of two binary variables: one that controls the appliance status and one recording the appliance start-up. In fact, when the appliance activation is requested by the user, its scheduling is inserted into the timeline (t) within the forthcoming control period; its activation would depend on the following factors:

- Availability of RES (PV power);
- Availability of Storage (Battery);
- Grid reference profile;
- Cost of energy.

The appliance must be activated within a maximum period of 24 h after its request. The ones with the shortest time to reach the 24 h' period would have higher priority.

Specific constraints have been added, as follows:

- The appliance can be activated only once a day (if used);
- The dryer can only be activated after the washing machine cycle;
- The number of weekly uses of an appliance is defined on a statistic base;
- After an appliance is turned-on, the cycle cannot be turned-off.

The description of the matrixes used for the implementation of the method is reported in Appendix A.

The MPC concept allows to know in advance the behavior of the system during the control horizon. The knowledge (or forecast) of environmental parameters and the load requested by the house are essential information to predict production from RES and to estimate the load profile. Data provided by CNMCA (Italian Air Force Meteorological Service) [37] have been used for the radiation forecast in Rome/Italy; a weather station, mounted in the building of Industrial Engineering at the University of Rome "Tor Vergata", has been used to measure the actual environmental parameters to be used as input data for the HRES model.

As far as the load is concerned, its forecast does not take into account deferrable loads and typical profiles have been built by dedicated studies and through historical consumption data.

4. Case description

Three different test cases have been studied:

- A Standard Prosumer case where only LOAD, PV and GRID are considered;
- A MG controlled by means of a RBC strategy;
- A MG controlled by means of a MPC strategy.

For all the different cases the same base load profile has been chosen to have a fair comparison of results. In this way, in fact, the overall energy consumed is same for all the configurations analyzed.

Grid costs have been evaluated according to the Italian market prices for users in tariff D3 [38]. Electricity cost is 0.30 €/kWh when withdrawals occur on weekdays from 8:00 am to 7:00 pm (F1 period), otherwise it is 0.25 €/kWh (F2/F3 period[1]), tax included. The unbalance value depends on several factors depending on local issues, and thus for this study, the unbalance values have been restricted to energy amounts expressed in kWh, assuming the value of 0.195 €/kWh as suggested in [39]. Standard commercial battery costs have been evaluated for the battery pack at 1000 €/KWh with a duability of about 10,000 cycles. Fuel costs have been assumed at 0.8 €/Scm, with a heating value of 9.6 kWh/Scm, resulting in a price of 0.0833 €/kWhe produced by the fuel cell. A PEM FC system of 1.2 kW with a durability of 6000 h and capital costs of about 14.000€ has been considered and stack replacement costs of about 3000€. Moreover, the number of fuel cell starts and stops strongly affects the fuel cell durability, and

[1] F2 from 7 a.m. to 8 a.m. and from 7 p.m. to 11 p.m. weekdays – and from 7 a.m. to 11 p.m. over the weekend; while F3 from 12 p.m. to 7 a.m. and from 11 p.m. to 12 p.m. from Monday to Saturday and all over the Sunday and Holidays.

therefore, every FC shutdown has been assumed affecting the lifetime by 3 steady hours operation time [31].

5. Results: Comparison of Control Strategies

The amount of energy exchanged with the grid for the three different strategies for each time cost zone is shown in Fig. 6. The MPC allows reducing the energy fluxes with the grid, and in particular the energy consumed during the F1 (most expensive) period of the day. In the case of the standard prosumer, the PV energy is hardly consumed as testified by the almost even balance between energy sold and purchased from the grid. The use of storage system already improves performance with the baseline RBC strategy, and even better benefits are demonstrated by using MPC features thanks to load scheduling and weather/load forecasts. In detail, an overall reduction of 42% and 10.5% has been achieved using the MPC strategy if compared with the Standard Prosumer and the RBC strategy respectively. The reduction is mainly obtained within the more expensive F1 period (almost 71% for both the strategies against the Standard Prosumer).

Moreover, the HRES solutions gave a greater amount of the self-consumed energy quota produced by local RES with a consequent reduction of the energy sold to the grid for both the proposed strategies. The increase is in the order of 50% for the RBC if compared with the Standard Prosumer, with an additional 8.5% of the MPC strategy if compared with the RBC case.

Power profiles are provided in Figs. 7–9 for the three different cases tested referring to one of the simulated days in order to explain the behavior. The standard prosumer consumes energy at the expense of the grid whenever a demand of energy arises, and thus even a small over-production from PV cannot be self-consumed, as well as the excess is given to the grid. As the RBC strategy does not feature any forecast of system trajectory over time (Fig. 8), the grid reference ideally exchanged with the grid (GRID ref) and load profiles do not match, showing inefficiencies in the use of the storage system that transfers fluctuations of production from RES to the grid once it is fully charged or fully discharged.

The use of the MPC strategy (Fig. 9) allows to reduce and smooth the energy exchange profile with the grid, thus not overloading it and absorbing the fluctuations over time of load and RES production profiles. The profiles of energy purchased/sold from/to the grid are plotted over time in Figs. 10–12 to further clarify the mechanism. Consumptions are effectively moved by the MPC strategy toward night hours, or whenever there is an excess of production from RES, in order to better match the reference profile. Energy consumptions not attending the GRID Reference profile are thus discouraged.

6. Results: effect of MPC control strategy on sizing

Once the benefits of the MPC have been highlighted in terms of prosumer-grid interaction the analysis has been extended to study the effect of the control strategy on system sizing. Different values of PV peak power, FC peak power and Battery Energy Storage System (BESS) capacity have been tested in order to analyze the benefits of implementing a MPC strategy compared to the RBC one. In order to have more general parameters, all the components sizes have been reduced to a dimensionless form referring to load consumption. In particular, three indexes have been used for the PV system, FC system and BESS sizes, defined as:

$$I_{size} = \frac{E^*_{PV}}{E_{LOAD_y}}$$

$$BESS_{size} = \frac{E_{BESS}}{E_{LOAD_{avg}}}$$

$$FC_{size} = \frac{P_{FC}}{P_{LOAD_{avg}}}$$

where E^*_{PV} is the theoretical energy that can be produced over one year by the considered PV plant, E_{LOAD_y} is the total energy consumed by the load over one year, E_{BESS} is the energy stored the BESS, $E_{LOAD_{avg}}$ is the average daily energy consumption, P_{FC} is the power of the installed FC and $P_{LOAD_{avg}}$ is the average daily power of the load.

According to the definitions provided, greater index values correspond to subsystem oversizings if compared with the energy consumed at the load.

Figs. 13–22 show different performance parameters of the HRES as functions of the subsystem size and control strategy. For both the control strategies tested, for each of the four different I_{size} evaluated (19.5556; 31.28896; 46.9334; 70.4), 12 monthly simulations have been run by varying $BESS_{size}$ and FC_{size} ranging between 0.6587–2.6348 and 2.4701–5.8184 respectively (in detail 0.6587; 1.2938; 1.9255; 2.6348 for the BESS size and 2.4701; 3.6368; 5.8184 for the FC size). A total number of 96 cases for each month have been carried out.

Results have been summarized in the surface plots (see following Figs. 13–22 and Tables 1–10) to show the impact of the control strategy on system performance under different components' sizing.

Fig. 13 shows the energy purchased from the grid for each design combination tested for both RBC (red) and MPC/MILP (purple) strategies for the month of January (Winter – left) and the month of July (Summer – right) at the lowest I_{size} considered. It can be noted in the plots that the MPC strategy offers benefits in terms of energy purchased, especially during the winter period. In fact, with low radiation, the capability of forecasting the weather and the load profile helps controlling more effectively the storage system. On the other hand, the RBC control strategy that is based only on instant control actions gives saturation with respect to battery capacity already at the smallest BESS sizes. Further advantages, although of lesser quantitative importance, can be noted for the summer case where the MPC gives a reduction of the energy purchased from the grid for all the systems considered. However, in this case, greater BESS capacity values may be used effectively also with a RBC strategy. For both the strategies, the effect of the FC on the energy purchased from the grid is quite negligible as the

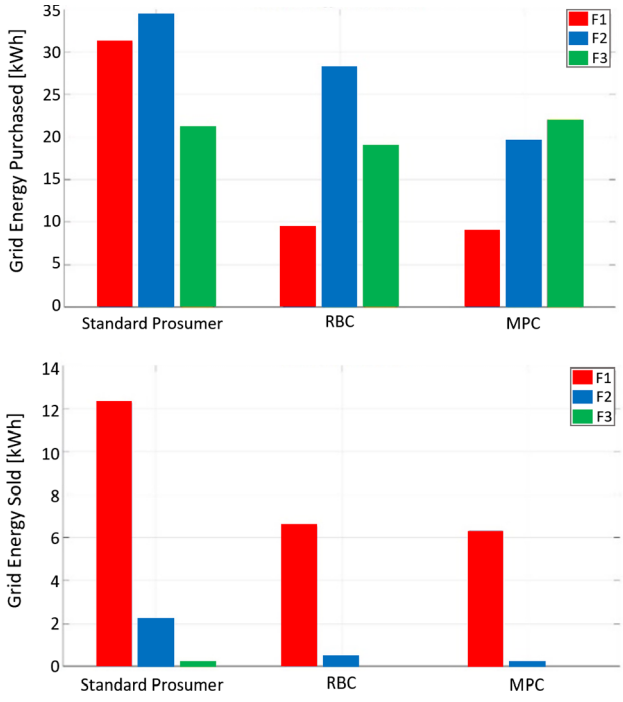

Fig. 6. Amount of energy purchased from GRID per strategy (top), amount of energy sold to GRID per strategy (bottom).

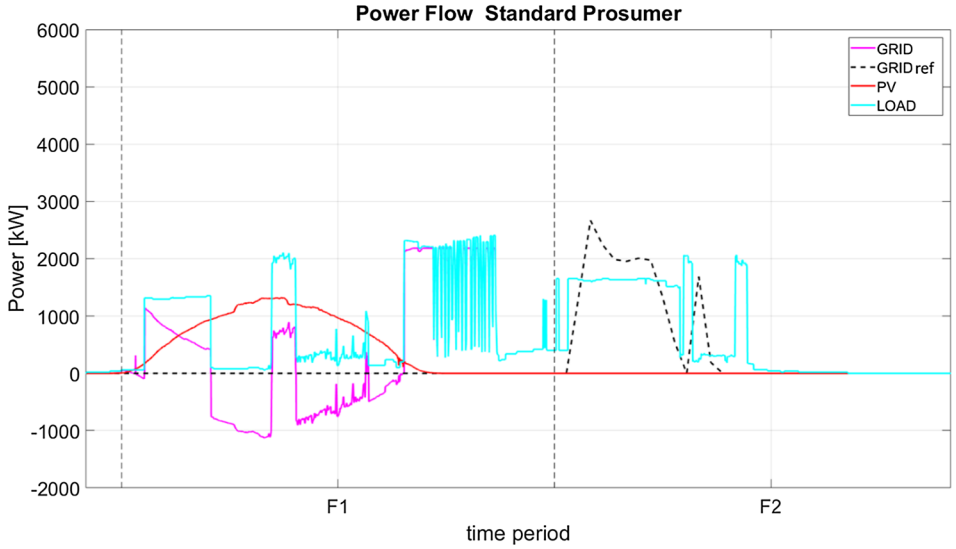

Fig. 7. Power profile of LOAD demand, PV production and actual power exchanged with the grid compared against the GRID reference – Standard prosumer case.

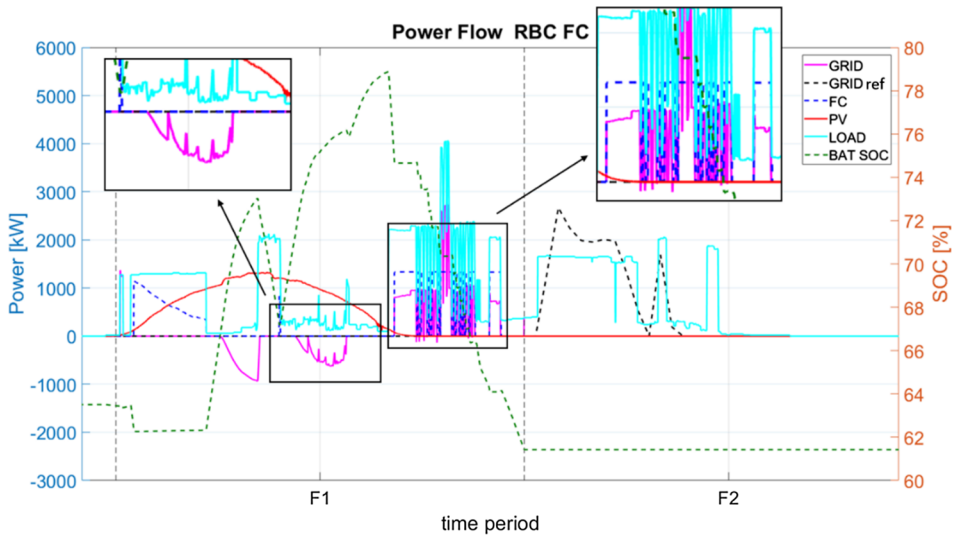

Fig. 8. Power profile of LOAD demand, PV production, FC production and actual power exchanged with the grid compared against the GRID reference, on the right axis the Battery State of Charge – RBC case.

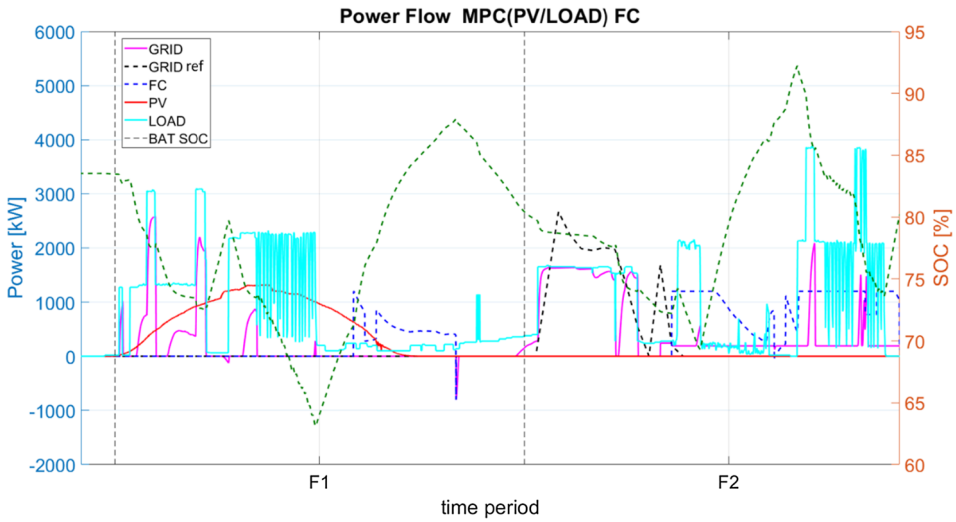

Fig. 9. Power profile of LOAD demand, PV production, FC production and actual power exchanged with the grid compared against the GRID reference, on the right axis the Battery State of Charge – MPC case.

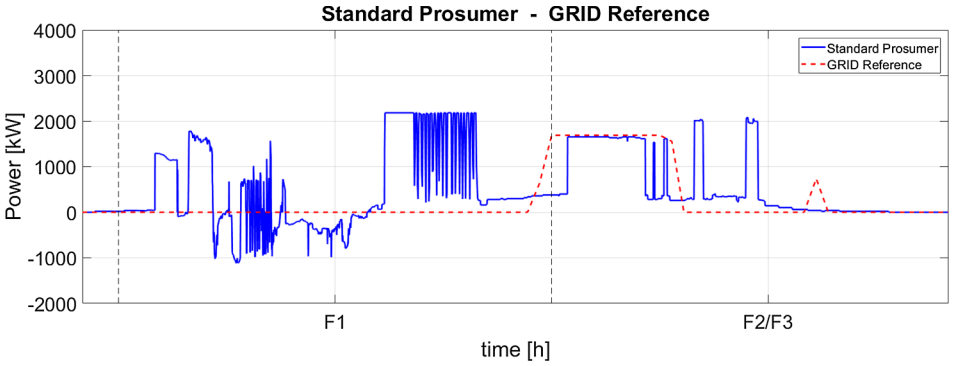

Fig. 10. Standard Prosumer grid exchanged profile vs reference profile.

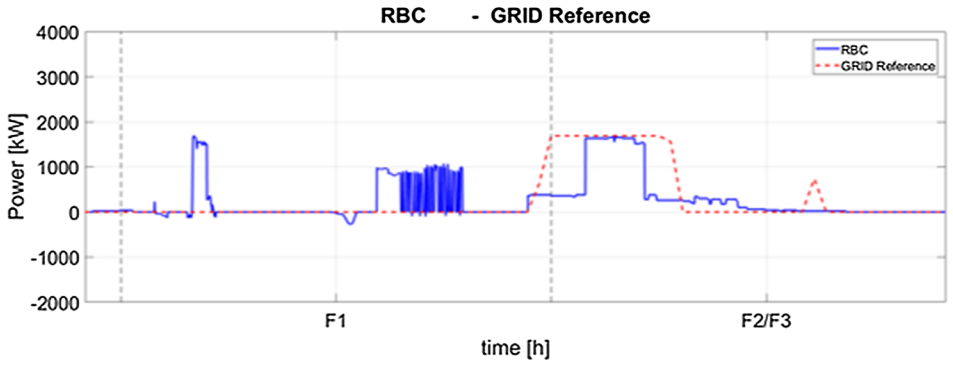

Fig. 11. RBC grid exchanged profile vs energy vs reference profile.

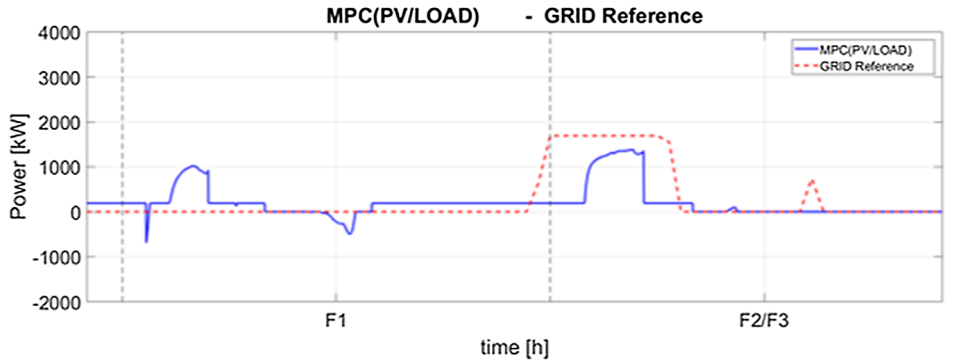

Fig. 12. MPC grid exchanged profile vs reference profile.

energy produced by the FC is more expensive than the energy purchased from the grid for most of the time. The FC plays on the other hand a key role for the stabilization of fluctuations of the energy exchanged with the grid and, thanks to the more effective utilization of the BESS with the MPC strategy, it can be downsized with evident economic advantages.

Moving towards the higher I_{size} values (Fig. 14), similar considerations can be drawn. In general, a reduction of the energy purchased from the grid may be obtained for both the control strategies; also in this case, the MPC allows for a maximization of the storage effectiveness as the energy purchased is reduced. A slight decrease of the energy purchased can be noted also for the RBC case in winter; however, due to the relevant uncertainties of weather conditions in such cases, the BESS capacity cannot be exploited at the utmost with the RBC strategy.

The benefits of forecasting both weather and load for the MPC strategy in comparison with the RBC one, can also be noted looking at the energy stored and supplied by the BESS for the months of January and July at same PV plant sizes shown so far (Figs. 15–18).

Fig. 15 – on the left – confirms the predictions looking at the energy purchased by the grid on the BESS capacity utilization; increasing the BESS size does not affect the energy stored due to failure of the RBC strategy to compensate for the weather uncertainties. Without these capabilities the system is not able to maintain a minimum capacitance available at the battery whenever the radiation energy is available. With greater availability of radiation energy (during the summer case – on the right), BESS capacitance is exploited more effectively, although the positive effects of the MPC strategy are still evident.

Similar considerations can be drawn for the winter case at the highest I_{size} (Fig. 16 – left) values, while for the summer case at the same PV sizing a different trend can be noted. At the smaller BESS sizes the energy stored is greater for the RBC strategy than for the MPC one. This can be explained by the application of the DR strategy for the MPC to move over time specific deferrable loads in periods of time where the power can be produced and consumed by the prosumer simultaneously.

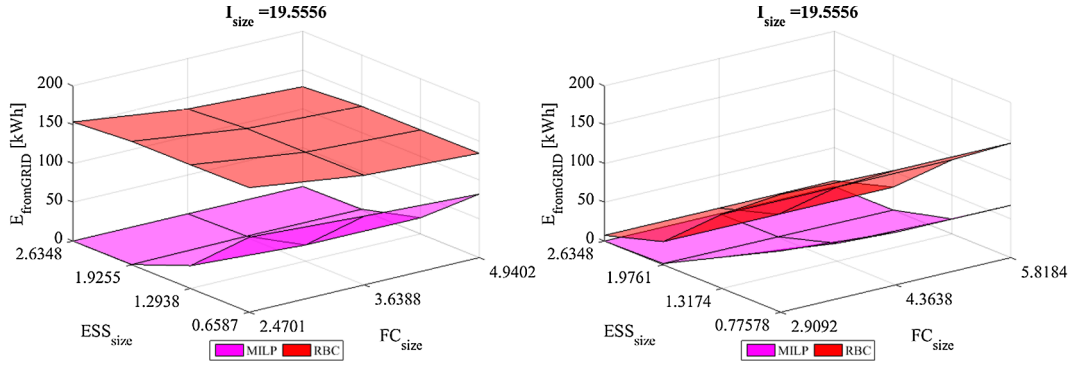

Fig. 13. Energy purchased by the grid for each design combination for both RBC and MPC/MILP strategies for the Winter (left) and the Summer (right) cases at the lowest I_{size}.

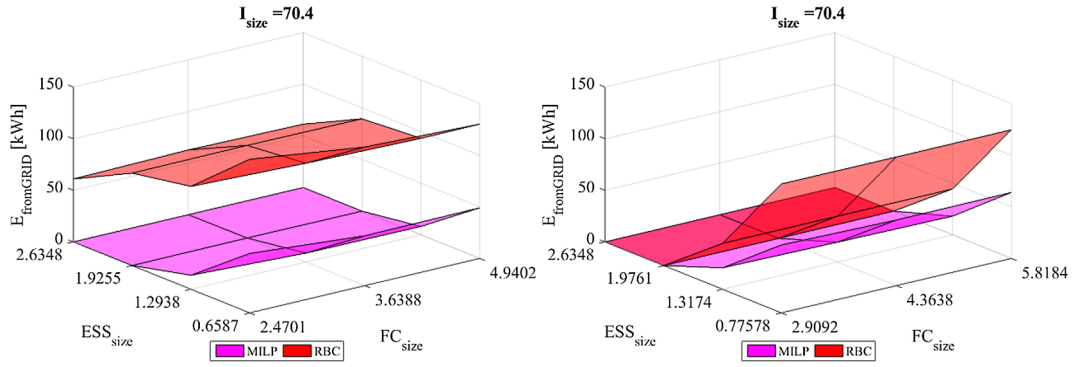

Fig. 14. Energy purchased by the grid for each design combination for both RBC and MPC/MILP strategies for the Winter (left) and the Summer (right) cases at the highest I_{size}.

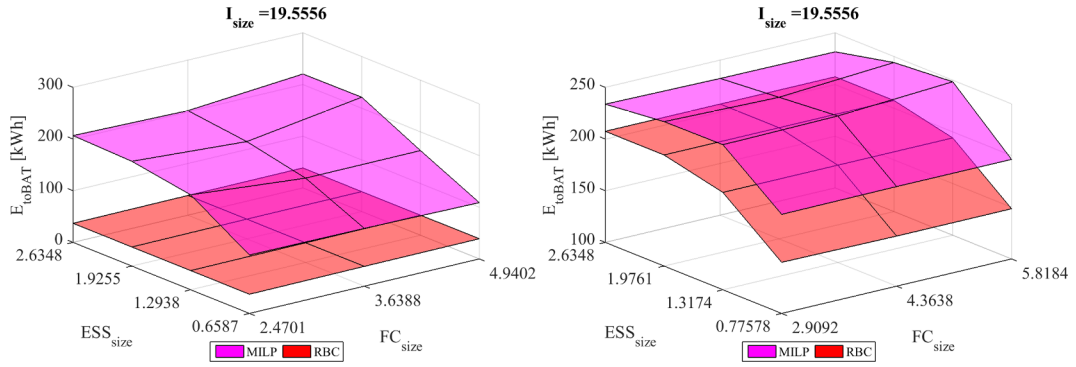

Fig. 15. Energy stored in the battery system for each design combination for both RBC and MPC/MILP strategies for the Winter (left) and the Summer (right) cases at the lowest $_{Isize}$.

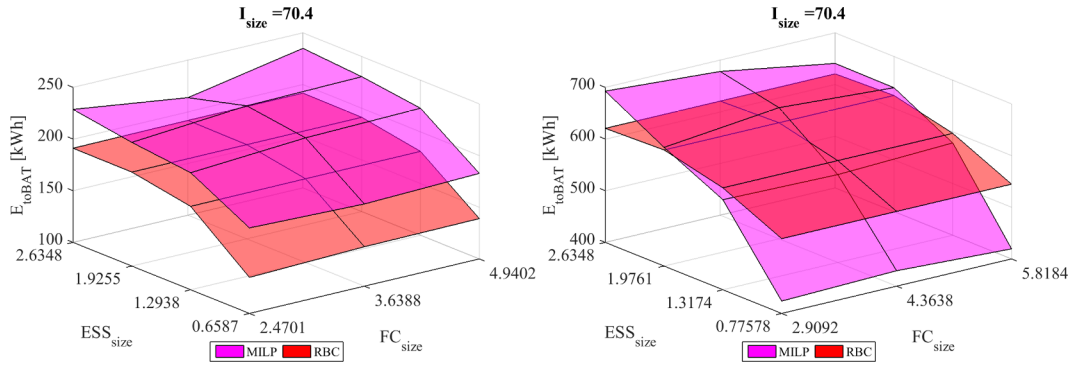

Fig. 16. Energy stored in the battery system for each design combination for both RBC and MPC/MILP strategies for the Winter (left) and the Summer (right) cases at the highest I_{size}.

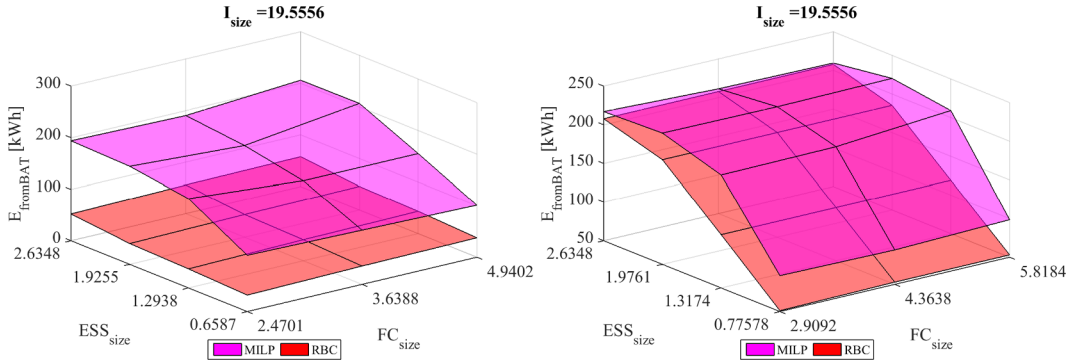

Fig. 17. Energy supplied by the battery storage system for each design combination for both RBC and MPC/MILP strategies for the Winter (left) and the Summer (right) cases at the lowest I_{size}.

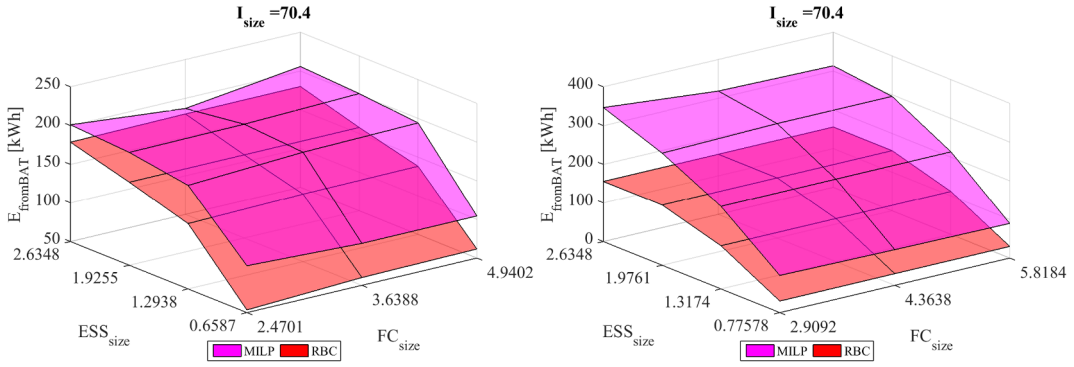

Fig. 18. Energy supplied by the battery storage system for each design combination for both RBC and MPC/MILP strategies for the Winter (left) and the Summer (right) cases at the highest I_{size}.

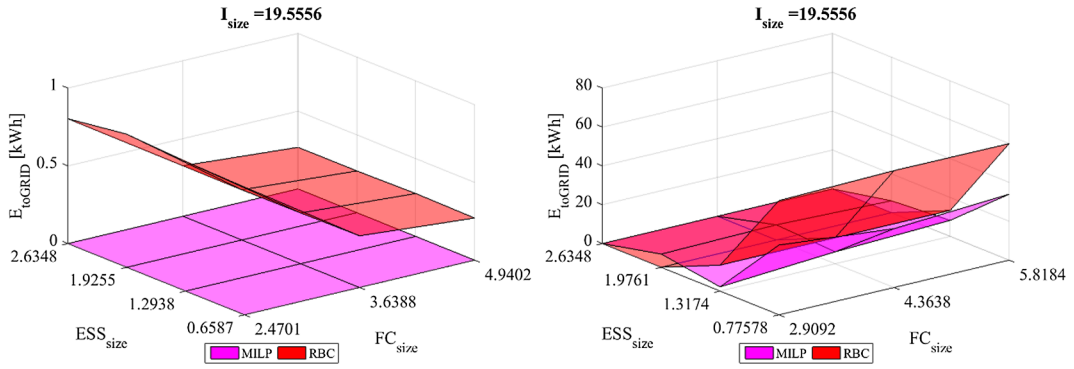

Fig. 19. Energy sold to the main grid for each design combination for both RBC and MPC/MILP strategies for the Winter (left) and the Summer (right) cases at the lowest I_{size}.

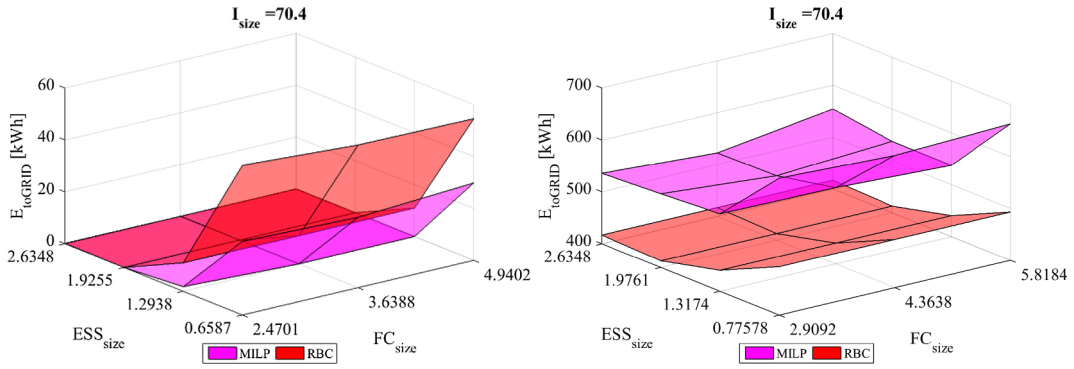

Fig. 20. Energy sold to the main grid for each design combination for both RBC and MPC/MILP strategies for the Winter (left) and the Summer (right) cases at the highest I_{size}.

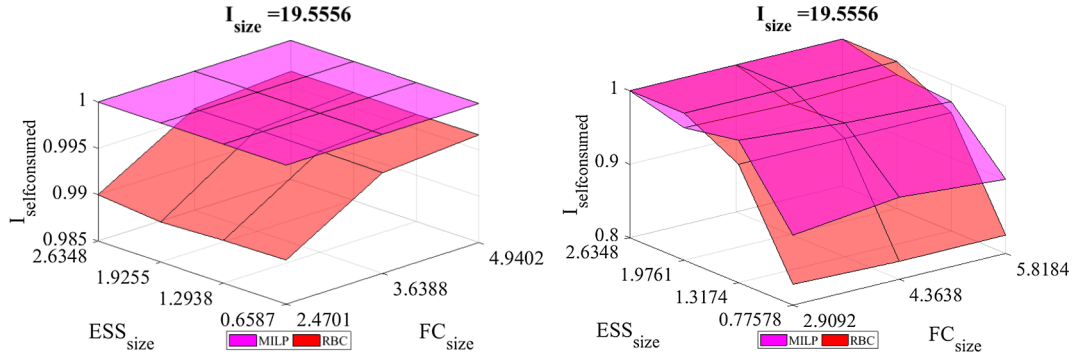

Fig. 21. Self-consumed index for each design combination for both RBC and MPC/MILP strategies for the Winter (left) and the Summer (right) cases at the lowest I_{size}.

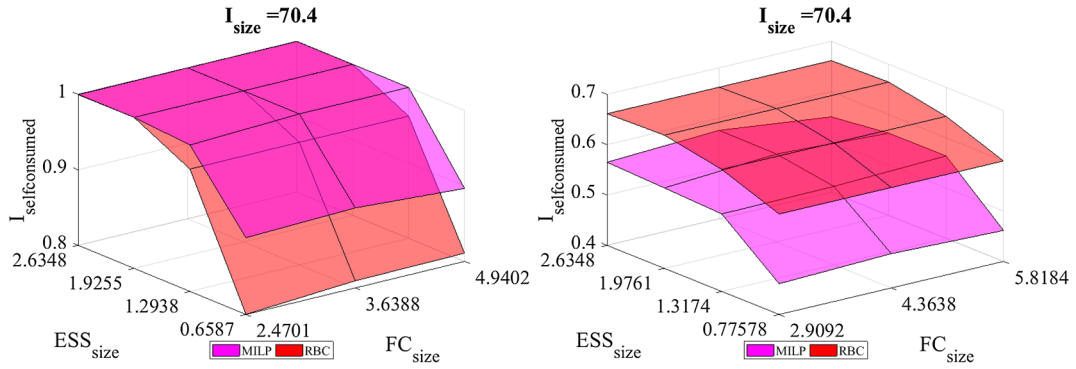

Fig. 22. Self-consumed index for each design combination for both RBC and MPC/MILP strategies for the Winter (left) and the Summer (right) cases at the highest I_{size}.

Table 1
Energy purchased by the main grid for each design combination for both RBC (red) and MPC/MILP (purple) strategies for the Winter (top) and the Summer (bottom) cases at the lowest I_{size}.

Energy from Grid [kWh] – left RBC | right MPC - Winter					
I_size = 19.5556		BESS_size			
		0.6587	1.2938	1.9255	2.6348
FC_size	2.4701	160.4 | 96.60	159.3 | 29.35	159.0 | 0.304	153.4 | 0
	3.6388	141.2 | 88.58	140.5 | 20.84	140.4 | 1.703	135.1 | 0
	4.9402	134.4 | 81.77	133.9 | 20.78	133.9 | 1.290	128.5 | 0
Energy from Grid [kWh] – left RBC | right MPC - Summer					
I_size = 19.5556		BESS_size			
		0.7758	1.3174	1.9761	2.6348
FC_size	2.9092	151.9 | 78.87	95.64 | 40.26	29.76 | 1.547	7.338 | 0
	4.3638	147.9 | 67.82	95.55 | 23.02	29.76 | 0.886	7.338 | 0
	5.8184	147.4 | 67.38	95.47 | 19.30	29.76 | 0.205	7.338 | 0

Table 2
Energy purchased by the main grid for each design combination for both RBC (red) and MPC/MILP (violet) strategies for the Winter (top) and the Summer (bottom) cases at the highest Isize.

Energy from Grid [kWh] – left RBC | right MPC - Winter					
I_size = 70.4		BESS_size			
		0.6587	1.2938	1.9255	2.6348
FC_size	2.4701	148.8 | 57.56	99.58 | 13.53	89.54 | 0.053	60.96 | 0
	3.6388	134.3 | 48.30	95.70 | 8.651	90.03 | 0.367	62.70 | 0
	4.9402	130.1 | 49.01	93.40 | 8.077	89.46 | 0.000	61.33 | 0
Energy from Grid [kWh] – left RBC | right MPC - Summer					
I_size = 70.4		BESS_size			
		0.7758	1.3174	1.9761	2.6348
FC_size	2.9092	124.9 | 65.78	44.41 | 20.72	0 | 0	0 | 0
	4.3638	124.6 | 63.58	44.41 | 19.19	0 | 0	0 | 0
	5.8184	124.6 | 63.91	44.41 | 18.05	0 | 0	0 | 0

Going towards greater BESS sizes, this effect is hidden by the greater BESS capacitance. Moreover, taking into account all the operating costs considered in the optimization process, part of the energy produced from RES is directly sold to the grid in the cheaper periods.

All the considerations stated so far can be straightened looking at the BESS to supply energy the load (Figs. 17 and 18). In all the cases, the MPC allows for having a more effective use of the BESS maximizing RES production as well.

A general trend for the reduction of the energy sold to the grid can be noted for both the control strategies referring to the whole set of design cases (Figs. 19 and 20). However, the occurrence of rather different trends is evident for each case studied. Looking at the winter case for the lower PV plant size, it can be noted that the MPC allows for a complete self-consumption of the energy produced from RES for all the BESS and FC sizes tested. This has two different positive effects: from one hand it may promote RES penetration with a greater production. From the other hand it helps minimizing the grid overload decreasing the investment on grid infrastructures.

Similar considerations can be done for the summer case at the lowest I_{size} and the winter case at the highest I_{size}. For both the cases the MPC allowed for a minimization of the energy sold to the grid enhancing the self-consumption index of the MG system. A threshold value is

Table 3
Energy stored in the battery storage system for each design combination for both RBC (red) and MPC/MILP (violet) strategies for the Winter (top) and the Summer (bottom) cases at the lowest Isize.

Energy to BESS [kWh] – left RBC | right MPC - Winter					
I_size = 19.5556		BESS_size			
		0.6587	1.2938	1.9255	2.6348
FC_size	2.4701	37.13 | 113.0	37.04 | 183.7	36.95 | 202.7	36.89 | 206.6
	3.6388	38.34 | 111.7	38.12 | 163.2	38.11 | 188.2	38.08 | 202.2
	4.9402	39.05 | 108.9	38.80 | 163.8	38.60 | 221.3	38.61 | 220.3
Energy to BESS [kWh] – left RBC | right MPC - Summer					
I_size = 19.5556		BESS_size			
		0.7758	1.3174	1.9761	2.6348
FC_size	2.9092	149.5 | 195.8	194.2 | 240.3	207.5 | 239.7	207.5 | 233.7
	4.3638	148.4 | 196.4	194.2 | 241.8	207.5 | 236.9	207.5 | 232.2
	5.8184	148.5 | 196.3	194.2 | 248.5	207.5 | 244.2	207.5 | 231.6

Table 4
Energy stored in the battery storage system for each design combination for both RBC (red) and MPC/MILP (violet) strategies for the Winter (top) and the Summer (bottom) cases at the highest Isize.

Energy to BESS [kWh] – left RBC | right MPC - Winter					
I_size = 70.4		BESS_size			
		0.6587	1.2938	1.9255	2.6348
FC_size	2.4701	134.9 | 182.7	180.7 | 213.2	190.9 | 219.7	191.1 | 228.6
	3.6388	138.1 | 179.5	181.0 | 220.6	191.1 | 228.6	191.6 | 213.6
	4.9402	139.0 | 182.7	181.1 | 222.9	191.2 | 230.5	191.7 | 235.0
Energy to BESS [kWh] – left RBC | right MPC - Summer					
I_size = 70.4		BESS_size			
		0.7758	1.3174	1.9761	2.6348
FC_size	2.9092	544.6 | 423.9	597.2 | 574.2	624.6 | 629.7	620.6 | 692.6
	4.3638	544.6 | 429.8	597.2 | 570.1	624.6 | 653.7	620.6 | 678.0
	5.8184	544.6 | 419.5	597.2 | 578.6	624.6 | 639.7	620.6 | 640.8

Table 5
Energy supplied by the battery storage system for each design combination for both RBC (red) and MPC/MILP (violet) strategies for the Winter (top) and the Summer (bottom) cases at the lowest Isize.

Energy from BESS [kWh] – left RBC | right MPC - Winter					
I_size = 19.5556		BESS_size			
		0.6587	1.2938	1.9255	2.6348
FC_size	2.4701	31.91 | 109.1	36.99 | 173.4	40.35 | 190.3	52.01 | 193.9
	3.6388	35.58 | 105.3	40.87 | 155.4	44.08 | 177.9	55.78 | 190.1
	4.9402	37.67 | 101.2	43.40 | 155.4	46.13 | 206.8	57.66 | 206.0
Energy from BESS [kWh] – left RBC | right MPC - Summer					
I_size = 19.5556		BESS_size			
		0.7758	1.3174	1.9761	2.6348
FC_size	2.9092	51.17 | 96.47	118.9 | 196.1	185.4 | 219.8	207.8 | 217.0
	4.3638	52.90 | 94.55	118.9 | 197.5	185.4 | 218.7	207.8 | 211.4
	5.8184	53.02 | 98.57	118.9 | 209.2	185.4 | 220.2	207.8 | 209.6

Table 6
Energy supplied by the battery storage system for each design combination for both RBC (red) and MPC/MILP (purple) strategies for the Winter (top) and the Summer (bottom) cases at the highest Isize.

Energy from BESS [kWh] – left RBC | right MPC - Winter					
I_size = 70.4		BESS_size			
		0.6587	1.2938	1.9255	2.6348
FC_size	2.4701	53.45 | 110.4	134.3 | 183.9	157.4 | 195.9	178.6 | 201.0
	3.6388	60.07 | 104.1	137.3 | 191.6	157.6 | 197.2	179.9 | 186.9
	4.9402	61.71 | 104.3	138.3 | 194.2	157.8 | 201.5	180.1 | 205.8
Energy from BESS [kWh] – left RBC | right MPC - Summer					
I_size = 70.4		BESS_size			
		0.7758	1.3174	1.9761	2.6348
FC_size	2.9092	29.77 | 95.82	111.3 | 213.3	155.7 | 289.9	155.7 | 346.5
	4.3638	30.06 | 92.01	111.3 | 213.6	155.7 | 295.9	155.7 | 318.7
	5.8184	30.06 | 89.45	111.3 | 213.8	155.7 | 295.8	155.7 | 313.4

Table 7
Energy sold to the main grid for each design combination for both RBC (red) and MPC/MILP (purple) strategies for the Winter (top) and the Summer (bottom) cases at the lowest Isize.

Energy to Grid [kWh] – left RBC | right MPC - Winter					
I_size = 19.5556		BESS_size			
		0.6587	1.2938	1.9255	2.6348
FC_size	2.4701	0.821 | 0	0.833 | 0	0.856 | 0	0.803 | 0
	3.6388	0.332 | 0	0.327 | 0	0.323 | 0	0.325 | 0
	4.9402	0.271 | 0	0.276 | 0	0.268 0	0.268 | 0
Energy to Grid [kWh] – left RBC | right MPC - Summer					
I_size = 19.5556		BESS_size			
		0.7758	1.3174	1.9761	2.6348
FC_size	2.9092	58.75 | 35.88	13.34 | 2.167	0 | 6.811	0 | 0
	4.3638	60.12 | 30.24	13.36 | 6.128	0 | 7.784	0 | 0
	5.8184	59.92 | 33.93	13.36 | 8.252	0 | 6.110	0 | 0

Table 8
Energy sold to the main grid for each design combination for both RBC (red) and MPC/MILP (purple) strategies for the Winter (top) and the Summer (bottom) cases at the highest Isize.

Energy to Grid [kWh] – left RBC | right MPC - Winter					
I_size = 70.4		BESS_size			
		0.6587	1.2938	1.9255	2.6348
FC_size	2.4701	57.67 | 28.38	10.96 | 1.750	0.006 | 0	0.140 | 0
	3.6388	54.98 | 27.11	10.84 | 0.000	0.009 | 0	0.028 | 0
	4.9402	54.57 | 29.82	10.99 | 0.000	0.019 | 0	0.067 | 0
Energy to Grid [kWh] – left RBC | right MPC - Summer					
I_size = 70.4		BESS_size			
		0.7758	1.3174	1.9761	2.6348
FC_size	2.9092	493.1 | 663.7	440.4 | 549.3	412.9 | 542.1	416.9 | 535.6
	4.3638	493.1 | 655.0	440.4 | 546.8	412.9 | 524.0	416.9 | 522.5
	5.8184	493.1 | 663.2	440.4 | 537.3	412.9 | 537.9	416.9 | 554.4

Table 9
Self-consumed index for each design combination for both RBC (red) and MPC/MILP (violet) strategies for the Winter (top) and the Summer (bottom) cases at the lowest Isize.

I selfconsumed [–] – left RBC | right MPC - Winter					
I_size = 19.5556		BESS_size			
		0.6587	1.2938	1.9255	2.6348
FC_size	2.4701	0.9898 | 1.0	0.9896 | 1.0	0.9893 | 1.0	0.9900 | 1.0
	3.6388	0.9959 | 1.0	0.9959 | 1.0	0.9960 | 1.0	0.9959 | 1.0
	4.9402	0.9966 | 1.0	0.9966 | 1.0	0.9967 | 1.0	0.9967 | 1.0
I selfconsumed [–] – left RBC | right MPC - Summer					
I_size = 19.5556		BESS_size			
		0.7758	1.3174	1.9761	2.6348
FC_size	2.9092	0.8283 | 0.8951	0.9610 | 0.9937	1.0 | 0.9801	1.0 | 1.0
	4.3638	0.8243 | 0.9116	0.9609 | 0.9821	1.0 | 0.9772	1.0 | 1.0
	5.8184	0.8248 | 0.9008	0.9610 | 0.9759	1.0 | 0.9821	1.0 | 1.0

evident, above which, further increasing the BESS capacity, the energy sold to the grid would be null. This design value is almost coincident for both the control strategies.

An inversion of the trends commented can be noted for the summer case at the higher I_{size}. In this scenario the minimization of the cost function gives an inversion of the behavior of the system increasing the energy flux to the grid during the cheaper periods. This leads to a general greater value for the energy sold to the grid for the MPC strategy if compared to the RBC one.

Complementary considerations can be drawn looking at the self-consumption index for the cases studied where the previous explanations are confirmed by the reported trends (Figs. 21 and 22).

7. Conclusions

In this paper the behavior of Hybrid Renewable Energy Systems (HRESs) has been discussed, with special regard to the features of integrating the production from Renewable Energy Sources (RES) with storage systems and Fuel Cells (FCs) and to the final aim of enabling a greater penetration of the Distributed Generation concept over the grid.

In particular, the energy management strategy to control the power splitting among the different subsystems is key to get the most out of HRES. Thus, the behavior of different system designs (in terms of power sizes of the subsystems) has been studied referring to two control strategies, namely RBC (Rule Based Control) and MPC (Model Predictive Control) ones.

The results obtained allow to support the following conclusions:

- The simple integration of power systems to produce energy from RES (typically PV systems) with battery systems and Fuel Cells, not featuring any advanced control strategies, does not allow to maximize the HRES performance giving a reduction of the overall energy stored in the BESS up to 160 kWh per week in winter or an increase of the energy purchased up to 150 kWh and 100 kWh per week respectively in winter and summer at low I_{size} with respect to the MPC strategy case.
- The Demand Side Management (DSM) feature, along with the implementation of the MPC, is essential to improve system effectiveness as the overall energy exchanged with the grid is, in fact, reduced of 42% and 10.5% for the energy purchased with respect to the Standard Prosumer and the RBC solution, and of the 54% and 8.5% for the energy sold if compared with the Standard Prosumer and the RBC cases respectively.
- HRESs featuring battery systems along with MPC strategy help reducing the fluctuations at the end-user providing further benefits for the grid operator.
- HRESs further featuring a FC system help mitigating grid unbalancing issues especially if operated with advanced control strategies.
- The use of rather simple control strategies based on rules (RBC), require oversizing of the different subsystems to have enough production from RES, and give in general an overuse of the FC thus increasing costs at equal level of performance. In the most favorable case, the energy stored in the BESS has been increased by 460% thanks to the use of the MPC strategy, with a consequent increase of the self-consumed quota of production and getting the energy purchased from the grid down to zero.

Table 10
Self-consumed index for each design combination for both RBC (red) and MPC/MILP (violet) strategies for the Winter (top) and the Summer (bottom) cases at the highest Isize.

I selfconsumed [–] – left RBC | right MPC - Winter					
I_size = 19.5556		BESS_size			
		0.6587	1.2938	1.9255	2.6348
FC_size	2.4701	0.8001 | 0.9017	0.9620 | 1.00	1.00 | 1.00	0.99 | 1.00
	3.6388	0.8095 | 1.000	0.9624 | 1.00	1.00 | 1.00	0.99 | 1.00
	4.9402	0.8109 | 1.000	0.9619 | 1.00	0.99 | 1.00	0.99 | 1.00
I selfconsumed [–] – left RBC | right MPC - Summer					
I_size = 19.5556		BESS_size			
		0.7758	1.3174	1.9761	2.6348
FC_size	2.9092	0.5996 | 0.4611	0.6424 | 0.5539	0.6647 | 0.5599	0.6615 | 0.5651
	4.3638	0.5996 | 0.4681	0.6424 | 0.5560	0.6647 | 0.5745	0.6615 | 0.5757
	5.8184	0.5996 | 0.4615	0.6424 | 0.5638	0.6647 | 0.5632	0.6615 | 0.5498

Appendix A

The objective function (4) is solved using the following canonical form

min $f^T X$

subjected to

$$\begin{cases} AX \le b \\ A_{eq}X = b_{eq} \\ L_b \le X \le U_b \end{cases}$$

where the vector X contains the control variables associated with the appliances, the grid, the battery and the fuel cell; the vector f^T is composed of the cost related to each control variable; L_b and U_b define the upper and lower limits for the values of the elements of X.

The linear equality constraint (3) can be represented by $A_{1,eq}X = b_{1,eq}$where

$$A_{1,eq} = [A_{wm,1}A_{dw,1}A_{d,1}A_{wm,2}A_{dw,2}\cdots A_{wm,n}A_{dw,n} - A_{\text{fromgrid}}A_{\text{togrid}}A_{ch} - A_{dch} - A_{fc}0\cdots 0]_{Nx((a+b+c)n+18N)}$$

$$b_{1,eq} = [E_{disp}]_{Nx1}$$

where

- N is the number of time steps a day
- A_{buy}, A_{sell}, A_{ch}, A_{dch}, A_{fc} are NxN identity matrices
- A_{wm}, A_{dw}, A_d are the shifting matrices of the n appliances with dimensions Nxa, Nxb, Nxc respectively. They are defined according to their power profile
- E_{disp} is defined as the difference between the energy production and the load.

The single activation a day of the appliances can be expressed by $A_{2,eq}X = b_{2,eq}$:

$$A_{2,eq} = \begin{bmatrix} A_{wm1,1} & 0 & 0 & 0 & \cdots & 0 & 0 & 0 & \cdots & 0 \\ 0 & A_{dw1,1} & 0 & 0 & \cdots & 0 & 0 & 0 & \cdots & 0 \\ 0 & 0 & A_{d1,1} & 0 & \cdots & 0 & 0 & 0 & \cdots & 0 \\ \vdots & \vdots & \vdots & \ddots & \vdots & \vdots & \vdots & \vdots & \ddots & \vdots \\ 0 & 0 & 0 & 0 & A_{wm1,n} & 0 & 0 & 0 & \cdots & 0 \\ \vdots & \vdots & \vdots & \vdots & 0 & A_{dw1,n} & 0 & 0 & \cdots & 0 \\ 0 & 0 & 0 & 0 & 0 & 0 & A_{d1,n} & 0 & \cdots & 0 \end{bmatrix}_{\text{nx((a+b+c)n+18N)}}$$

$$b_{2,eq} = \begin{bmatrix} \delta_{pr,1} \\ \delta_{pr,2} \\ \vdots \\ \delta_{pr,n} \end{bmatrix}_{nx1}$$

where

- $\delta_{pr}$is the binary variable representing the activation request of the user
- A_{wm1}, A_{dw1}, A_{d1} are ones' vectors of dimension a, b, c respectively

The energy balance of the battery can be expressed in the form $A_{3,eq}X = b_{3,eq}$:

$$A_{3,eq} = \begin{bmatrix} 0 & \cdots & 0 & \frac{A_{ch}}{E_c} & -\frac{A_{dch}}{E_c} & SOC & 0 & \cdots & 0 \end{bmatrix}_{Nx((a+b+c)n+18N)}$$

$$SOC = \begin{bmatrix} 1 & 0 & 0 & \cdots & 0 & 0 \\ -1 & 1 & 0 & \cdots & 0 & 0 \\ 0 & -1 & 1 & \cdots & 0 & 0 \\ \vdots & \vdots & \vdots & \ddots & \ddots & \vdots \\ 0 & 0 & 0 & 0 & -1 & 1 \end{bmatrix}_{NxN}$$

$$b_{3,eq} = \begin{bmatrix} -SOC_0 \\ 0 \\ \vdots \\ 0 \end{bmatrix}_{Nx1}$$

The equality constraints (9) can be represented as $A_{4,eq}X = b_{4,eq}$

$$\mathrm{A}_{4,\mathrm{eq}} = [0 \ \cdots \ 0 \ A_{fc,on/off} \ A_{fc,standby} \ -A_{fc,startup} \ A_{fc,shutdown} \ 0 \ \cdots \ 0]_{NX((a+b+c)n+18N)}$$

$$b_{4,eq} = \begin{bmatrix} 0 \\ \vdots \\ 0 \end{bmatrix}_{Nx1}$$

$$A_{fc,on-off} = \begin{bmatrix} 1 & 0 & 0 & \cdots & 0 & 0 \\ -1 & 1 & 0 & \cdots & 0 & 0 \\ 0 & -1 & 1 & \cdots & 0 & 0 \\ \vdots & \vdots & \vdots & \ddots & \ddots & \vdots \\ 0 & 0 & 0 & 0 & -1 & 1 \end{bmatrix}_{NxN} \qquad A_{fc,standby} = \begin{bmatrix} 1 & 0 & 0 & \cdots & 0 & 0 \\ -1 & 1 & 0 & \cdots & 0 & 0 \\ 0 & -1 & 1 & \cdots & 0 & 0 \\ \vdots & \vdots & \vdots & \ddots & \ddots & \vdots \\ 0 & 0 & 0 & 0 & -1 & 1 \end{bmatrix}_{NxN}$$

where $A_{fc,startup}$, $A_{fc,shutdown}$ are NxN identity matrices.

The definition of the power unbalance (14) is expressed by $A_{5,eq}X = b_{5,eq}$

$$A_{5,eq} = [0 \ \cdots \ 0 \ -A_{fromgrid} \ A_{togrid} \ 0 \ \cdots \ 0 \ A_{unb^+} \ -A_{unb^-}]_{Nx((a+b+c)n+18N)}$$

$$b_{5,eq} = [E_{grid\_ref}]_{Nx1}$$

where A_{unb^+}, A_{unb^-} are NxN identity matrices.

Then, the canonical linear equality constraint $A_{eq}X = b_{eq}$ becomes

$$\begin{bmatrix} A_{1,eq} \\ A_{2,eq} \\ A_{3,eq} \\ A_{4,eq} \\ A_{5,eq} \\ A_{6,eq} \end{bmatrix}_{(n+5N)x((a+b+c)n+18N)} \qquad X = \begin{bmatrix} b_{1,eq} \\ b_{2,eq} \\ b_{3,eq} \\ b_{4,eq} \\ b_{5,eq} \\ b_{6,eq} \end{bmatrix}_{(n+5N)x1}$$

In a similar way, the linear inequality constraints (6) and (7) can be represented by $A_1X \leq b_1$

$$A_1 = \begin{bmatrix} 0 & \cdots & 0 & A_{fc} & -E_{fc,max} & 0 & \cdots & 0 \\ 0 & \cdots & 0 & -A_{fc} & -E_{fc,min} & 0 & \cdots & 0 \end{bmatrix}_{2Nx((a+b+c)n+18N)}$$

$$b_1 = [0 \ \cdots \ 0]_{2Nx1}$$

where $E_{fc,max}$, $E_{fc,min}$ are NxN identity matrices.

Again, (10) and (11) can be expressed as $A_2X \leq b_2$

$$A_2 = \begin{bmatrix} 0 & \cdots & 0 & A_{fromgrid} & 0 & 0 & \cdots & 0 & -E_{A_{fromgrid},max} & 0 & 0 & \cdots & 0 \\ 0 & \cdots & 0 & 0 & A_{togrid} & 0 & \cdots & 0 & 0 & -E_{togrid,max} & 0 & \cdots & 0 \end{bmatrix}_{2Nx((a+b+c)n+18N)}$$

$$b_2 = [0 \ \cdots \ 0]_{2Nx1}$$

where $E_{fromgrid,max}$, $E_{togrid,max}$ are NxN identity matrices.

Mutual exclusive conditions (8) and (12) can be defined as $A_3X \leq b_3$ and $A_4X \leq b_4$ respectively

$$A_3 = [0 \ \cdots \ 0 \ A_{fc,on-off} \ A_{fc,standby} \ 0 \ \cdots \ 0]_{Nx((a+b+c)n+18N)}$$

$$A_4 = [0 \ \cdots \ 0 \ A_{buy} \ A_{sell} \ 0 \ \cdots \ 0]_{Nx((a+b+c)n+18N)}$$

$$b_3 = b_{4=}[1 \ \cdots \ 1]_{Nx1}$$

Then, the canonical linear inequality constraint $AX \leq b$ assumes the form

$$\begin{bmatrix} A_1 \\ A_2 \\ A_3 \\ A_4 \end{bmatrix}_{6Nx((a+b+c)n+18N)} \qquad X = \begin{bmatrix} b_1 \\ b_2 \\ b_3 \\ b_4 \end{bmatrix}_{6Nx1}$$

References

[1] Bajpai P, Dash V. Hybrid renewable energy systems for power generation in stand-alone applications: a review. Renew Sustain Energy Rev 2012;16(5):2926–39.

[2] IEA 2012 World Energy Outlook.

[3] Hatziargyriou N. Microgrid: architectures and control. Wiley; 2013.

[4] Thomas D, Deblecker O, Ioakimidis C. Optimal operation of an energy management system for a grid-connected smart building considering photovoltaics' uncertainty and stochastic electric vehicles' driving schedule. Appl Energy 2017. https://doi.org/10.1016/j.apenergy.2017.07.035.

[5] Liang H, Zhuang W. Stochastic modeling and optimization in a microgrid: a survey. Energies 2014;7:2027–50.

[6] Kolokotsa D, Rovas D, Kosmatopoulos E, Kalaitzakis K. A roadmap towards intelligent net zero- and positive-energy buildings. Sol Energy 2011;85(12):3067–84.

[7] Thomas D, Deblecker O, Bagheri A, Ioakimidis CS. A scheduling optimization model for minimizing the energy demand of a building using electric vehicles and a micro-turbine. 2016 IEEE international smart cities conference (ISC2). IEEE; 2016. p. 1–6.

[8] Zhou B, et al. Smart home energy management systems: concept, configurations, and scheduling strategies. Renew Sustain Energy Rev 2016;61:30–40.

[9] Han Y, Chen W, Li Q. Energy management strategy based on multiple operating states for a photovoltaic/fuel cell/energy storage DC microgrid. Energies 2017;10:136.

[10] Khatibzadeh A, Besmi M, Mahabadi A, Reza Haghifam M. Multi-agent-based controller for voltage enhancement in AC/DC hybrid microgrid using energy storages. Energies 2017;10:169.

[11] Wang H, Wang T, Xie X, Ling Z, Gao G, Dong X. Optimal capacity configuration of a hybrid energy storage system for an isolated microgrid using quantum-behaved particle swarm optimization. Energies 2018;11:454.

[12] Moradi H, Esfahanian M, Abtahi A, Zilouchian A. Modeling a hybrid microgrid using probabilistic reconfiguration under system uncertainties. Energies 2017;10:1430.

[13] De Angelis F, et al. Optimal home energy management under dynamic electrical and thermal constraints. IEEE Trans Ind Inf 2013;9(3):1518–27.

[14] Özkan HA. A new real time home power management system. Energy Build 2015;97:56–64.

[15] Xue X, Wang S, Sun Y, Xiao F. An interactive building power demand management strategy for facilitating smart grid optimization. Appl Energy 2014;116:297–310.

[16] Pascual J, Sanchis P, Marroyo L. Implementation and control of a residential electrothermal microgrid based on renewable energies, a hybrid storage system and demand side management. Energies 2014;7:210–37.

[17] Yoo C-H, Chung I-Y, Lee H-J, Hong S-S. Intelligent control of battery energy storage

for multi-agent based microgrid energy management. Energies 2013;6:4956–79.
[18] Lim Y, Kim H-M, Kinoshita T. Distributed load-shedding system for agent-based autonomous microgrid operations. Energies 2014;7:385–401.
[19] Kim H-M, Lim Y, Kinoshita T. An intelligent multiagent system for autonomous microgrid operation. Energies 2012;5:3347–62.
[20] Tamalouzt S, Benyahia N, Rekioua T, Rekioua D, Abdessemed R. Performances analysis of WT-DFIG with PV and fuel cell hybrid power sources system associated with hydrogen storage hybrid energy system. Int J Hydrogen Energy 2016;41(45):21006–21.
[21] Bruni G, Cordiner S, Mulone V, Rocco V, Spagnolo F. A study on the energy management in domestic micro-grids based on Model Predictive Control strategies. Energy Convers Manage 2015;102:50–8. https://doi.org/10.1016/j.enconman.2015.01.067. ISSN 0196-8904.
[22] Wanjiru EM, Zhang L, Xia X. Model predictive control strategy of energy-water management in urban households. Appl Energy 179, 2016,:821–31. https://doi.org/10.1016/j.apenergy.2016.07.050. ISSN 0306-2619.
[23] Parisio A, Rikos E, Tzamalis G, Glielmo L. Use of model predictive control for experimental microgrid optimization. Appl Energy 2014;115:37–46. https://doi.org/10.1016/j.apenergy.2013.10.027. ISSN 0306-2619.
[24] Chen Z, Wu L, Fu Y. Real-time price-based demand response management for residential appliances via stochastic optimization and robust optimization. IEEE Trans Smart Grid 2012;3(4):1822–31.
[25] Erdinc O, Paterakis NG, Pappi IN, Bakirtzis AG, Catalão JP. A new perspective for sizing of distributed generation and energy storage for smart households under demand response. Appl Energy 2015;143:26–37.
[26] Dagdougui H, Minciardi R, Ouammi A, Robba M, Sacile R. Modeling and optimization of a hybrid system for the energy supply of a “Green” building. Energy Convers Manage 2012;64:351–63.
[27] Bianchini G, Casini M, Vicino A, Zarrilli D. Demand-response in building heating systems: a Model Predictive Control approach. Appl Energy 168, 2016,:159–70. https://doi.org/10.1016/j.apenergy.2016.01.088. ISSN 0306-2619.
[28] Fiorentini M, Wall J, Ma Z, Braslavsky JH, Cooper P. Hybrid model predictive control of a residential HVAC system with on-site thermal energy generation and storage. Appl Energy 2017;187:465–79. https://doi.org/10.1016/j.apenergy.2016.11.041. ISSN 0306-2619.
[29] Lu Y, Wang S, Sun Y, Yan C. Optimal scheduling of buildings with energy generation and thermal energy storage under dynamic electricity pricing using mixed-integer nonlinear programming. Appl Energy 2015;147:49–58.
[30] Bruni G, Cordiner S, Galeotti M, Mulone V, Nobile M, Rocco V. Control Strategy influence on the efficiency of a hybrid photovoltaic-battery-fuel cell system distributed generation system for domestic applications. Energy Procedia 2014;45:237–46. https://doi.org/10.1016/j.egypro.2014.01.026.
[31] Bartolucci L, Cordiner S, Mulone V, Rocco V, Rossi JL. Hybrid renewable energy systems for renewable integration in microgrids: influence of sizing on performance. Energy 2018;152:744–58. https://doi.org/10.1016/j.energy.2018.03.165.
[32] Mariani A. Energy efficiency for end-users: design and test of a micro-grid prototype. 2012. Ph.D. Dissertation.
[33] Bartolucci L, Cordiner S, Mulone V, et al. Renewable sources integration through the optimization of the load for residential applications. Energy Procedia 2017;142C:2208–13.
[34] Bruni G, Cordiner S, Mulone V. Domestic distributed power generation: effect of sizing and energy management strategy on the environmental efficiency of a photovoltaic-battery-fuel cell system. Energy 77, 2014,:133–43. https://doi.org/10.1016/j.energy.2014.05.062. ISSN 0360-5442.
[35] Cordiner S, Mulone V, Giordani A, et al. Fuel cell based hybrid renewable energy systems for off-grid telecom stations: data analysis from on field demonstration tests. Appl Energy 2017;192:508–18. https://doi.org/10.1016/j.apenergy.2016.08.162. ISSN 0306-2619.
[36] Bartolucci L, Cordiner S, Mulone V, Rocco V, Rossi JL. Renewable source penetration and microgrids: effects of MILP – based control strategies. Energy 2018;152:416–26. https://doi.org/10.1016/j.energy.2018.03.145.
[37] CNMCA. Homepage|MeteoAM.it – Air Force Weather Service; 2017. Available: <http://www.meteoam.it/>.
[38] AEEGSI <http://www.autorita.energia.it/it/index.htm>.
[39] Guandalini G, Campanari S, Romano MC. Power-to-gas plants and gas turbines for improved wind energy dispatchability: energy and economic assessment. Appl Energy 2015;147:117–30.